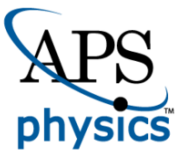

Tunable multiphonon blockade in coupled nanomechanical resonators

Adam Miranowicz, Jiří Bajer, Neill Lambert, Yu-xi Liu, and Franco Nori

Phys. Rev. A **93**, 013808 — Published 7 January 2016

DOI: 10.1103/PhysRevA.93.013808

Tunable multiphonon blockade in coupled nanomechanical resonators

Adam Miranowicz,[1,2] Jiří Bajer,[3] Neill Lambert,[2] Yu-xi Liu,[4,5,2] and Franco Nori[2,6]

[1]*Faculty of Physics, Adam Mickiewicz University, 61-614 Poznań, Poland*
[2]*CEMS, RIKEN, Wako-shi, Saitama 351-0198, Japan*
[3]*Department of Optics, Palacký University, 772 00 Olomouc, Czech Republic*
[4]*Institute of Microelectronics, Tsinghua University, Beijing 100084, China*
[5]*Tsinghua National Laboratory for Information Science and Technology (TNList), Beijing 100084, China*
[6]*Physics Department, The University of Michigan, Ann Arbor, Michigan 48109-1040, USA*

A single phonon in a nonlinear nanomechanical resonator (NAMR) can block the excitation of a second phonon [Phys. Rev. A**82**, 032101 (2010)]. This intrinsically quantum effect is called phonon blockade, and is an analog of Coulomb blockade and photon blockade. Here we predict tunable multiphonon blockade in coupled nonlinear NAMRs, where nonlinearity is induced by two-level systems (TLSs) assuming dispersive (far off-resonance) interactions. Specifically, we derive an effective Kerr-type interaction in a hybrid system consisting of two nonlinearly-interacting NAMRs coupled to two TLSs and driven by classical fields. The interaction between a given NAMR and a TLS is described by a Jaynes-Cummings-like model. We show that by properly tuning the frequency of the driving fields one can induce various types of phonon blockade, corresponding to the entangled phonon states of either two qubits, qutrit and quartit, or two qudits. Thus, a k-phonon Fock state (with $k = 1, 2, 3$) can impede the excitation of more phonons in a given NAMR, which we interpret as a k-phonon blockade (or, equivalently, phonon tunneling). Our results can be explained in terms of resonant transitions in the Fock space and via phase-space interference using the s-parametrized Cahill-Glauber quasiprobability distributions including the Wigner function. We study the nonclassicality, entanglement, and dimensionality of the blockaded phonon states during both dynamics and in the stationary limits.

PACS numbers: 85.85.+j, 03.65.Yz, 42.50.Dv

I. INTRODUCTION

Nanomechanical and optomechanical devices are a versatile technology [1–7], with a range of applications in the quantum regime [8]. Examples include small mass or weak-force detection [9–11], quantum measurements [12], and quantum-information processing. The first success in putting a mechanical device in a quantum state was performed [13] by purely cryogenic means, due to the frequency of the mechanical phonons [14] being larger than the thermal energy. Since then lower-frequency devices (which thus have larger mass) have been put in quantum states using side-band cooling via microwave and optical cavities [15–18]. These breakthroughs have been followed by the observation of state transfer [19–22] between an electromagnetic cavity and the mechanical system, with the goal of developing hybrid mechanical circuit devices [19, 23, 24] for applications in quantum technologies [25, 26].

Moving into the nonlinear regime with such quantum nanomechanical devices is desirable for several reasons: It will allow to observe highly nonclassical effects, as well as allowing to individually address different transitions within the mechanical system, so that it behaves as a mechanical artificial atom. In the realm of quantum optics [27–36] and circuit quantum electrodynamics [37–39], nonlinearities are typically associated with "photon blockade" (also referred to as the optical state truncation by quantum nonlinear scissors [40, 41]). In this regime the nonlinear nature of the spectrum of an optical cavity [42], induced via, e.g., a Kerr nonlinearity, means that the presence of a single photon within the cavity prevents the transmission of a second photon. In nonlinear mechanical systems one expects an analogous "phonon blockade" [43, 44] to arise. This requires either strong intrinsic nonlinearities [45], or induced nonlinearity via ancillary nonlinear systems (like qubits or artificial two-level systems [46]). Finally, while coupling between mechanical phonons and electromagnetic photons has been achieved in the quantum regime [47], the controlled coupling between multiple mechanical modes has so far been restricted to classical devices [48]. Such controllable coupling would enable the observation of entangled states [49–51], and the Bell inequality violation with massive objects [45], as well as the realization of coupled mechanical qubits [52, 53].

Our goal in this work is to study the combination of nonlinearity-induced phonon blockade effects via the coupling between the mechanical modes of NAMRs. We will show that the infinite-dimensional mechanical states of the NAMRs, under proper resonance conditions, can effectively be truncated to the states of finite-dimensional systems of either two coupled qubits, a three-level system (called a qutrit) coupled to a four-level system (referred to as quartit or ququart), or, in general, two coupled d-level systems (qudits).

While our model can be considered as a quantum limit of the classical systems studied in Ref. [54], we discuss explicitly how the nonlinearities can be tuned using an ancilla two-level system (TLS). We will show how this combination of phonon-blockade and two-NAMR (or two-mode) coupling leads to multiphonon blockade (or phonon tunneling), in analogy to the predictions of multiphoton blockade [55–58] and closely related photon tunneling [36, 58–60]. For example, Ref. [36] provides a pedagogical explanation of how photon blockade can lead to the observation of a single-photon tunneling effect in an analogous way to how Coulomb blockade can lead to the observation of single-electron tunneling.

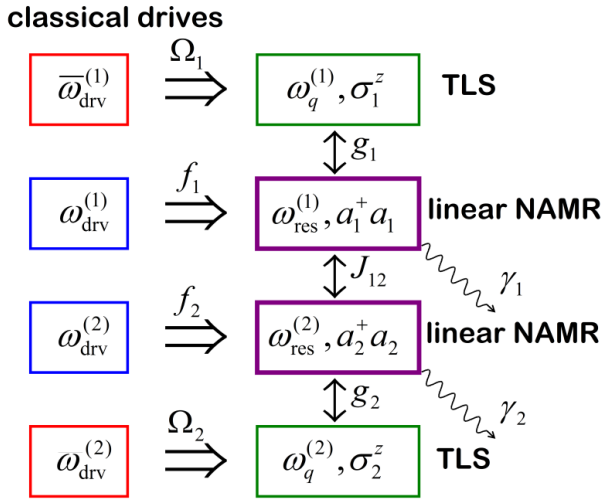

FIG. 1: (Color online) Schematic diagram for the couplings in the dissipative hybrid system described by the Hamiltonian given in Eq. (1). The system consists of two linear nanomechanical resonators (NAMRs), with frequencies $\omega^{(n)}_{\rm res}$, and a pair of two-level systems (TLSs), with frequencies $\omega^{(n)}_{\rm q}$, driven by classical fields, with frequencies $\omega^{(n)}_{\rm drv}$ and $\bar{\omega}^{(n)}_{\rm drv}$, respectively. Moreover, Ω_n, f_n, g_n, and J_{12} denote the coupling strengths of the depicted subsystems; γ_n are the NAMR decay rates; a_n ($a^\dagger_n$) is the phonon annihilation (creation) operator for the nth NAMR, and σ^z_n is the Pauli operator for the nth TLS.

We discuss here how the form of the multiphonon blockade can be tuned via driving, and verify the resultant highly nonclassical states with a variety of measures.

This paper is organized as follows: In Sec. II, we describe a model for a hybrid system of coupled linear NAMRs and TLSs. In this section and in Appendix A, we also show how a Kerr-type nonlinearity can be induced via NAMR-TLS interactions, and derive an effective Hamiltonian for the coupled nonlinear NAMRs. The possibility of observing multiphonon blockades in this system is described in Sec. III. We summarize several methods to assess nonclassicality, which we then apply in our analysis of phonon blockade in Secs. IV and V. We conclude in Sec. VI.

II. MODEL

A. Time-dependent Hamiltonian

We consider a hybrid system, as schematically depicted in Fig. 1, consisting of two interacting driven linear nanomechanical resonators (NAMRs), described by the Hamiltonian $H_{\rm res}$, coupled to two driven two-level systems (TLSs, qubits), given by the Hamiltonian $H_{\rm q}$. The interaction $H_{\rm JC}$ between the nth NAMR and nth TLS (for $n = 1, 2$) is described by a Jaynes-Cummings-like model under the rotating wave-approximation. The interaction $H_{\rm int}$ between the two NAMRs can be interpreted as a combined driven process of frequency conversion and parametric amplification [54]. Thus, the total microscopic Hamiltonian, representing the system shown in Fig. 1, reads (hereafter $\hbar = 1$ and $n = 1, 2$):

$$
\begin{aligned}
H &= H_{\rm res} + H_{\rm q} + H_{\rm JC} + H_{\rm int}, && (1)\\
H_{\rm res} &= \sum_n \omega^{(n)}_{\rm res} a^\dagger_n a_n + f_n\left[a_n \exp(i\omega^{(n)}_{\rm drv} t) + {\rm h.c.}\right], && (2)\\
H_{\rm q} &= \sum_n \frac{\omega^{(n)}_{\rm q}}{2}\sigma^z_n + \frac{\Omega_n}{2}\left[\sigma^-_n \exp(i\overline{\omega}^{(n)}_{\rm drv} t) + {\rm h.c.}\right], && (3)\\
H_{\rm JC} &= \sum_n g_n(a_n\sigma^+_n + a^\dagger_n\sigma^-_n), && (4)\\
H_{\rm int} &= J_{12}\left[a_1 \exp(i\omega^{(1)}_{\rm drv} t) + {\rm h.c.}\right] \\
&\quad \times \left[a_2 \exp(i\omega^{(2)}_{\rm drv} t) + {\rm h.c.}\right], && (5)
\end{aligned}
$$

where a_n and $a^\dagger_n$ are, respectively, the phonon annihilation and creation operators for the nth NAMR,

$$
\begin{aligned}
a_n &= (2m_n\omega^{(n)}_{\rm res})^{-1/2}(m_n\omega^{(n)}_{\rm res} x_n + ip_n),\\
a^\dagger_n &= (2m_n\omega^{(n)}_{\rm res})^{-1/2}(m_n\omega^{(n)}_{\rm res} x_n - ip_n), \qquad (6)
\end{aligned}
$$

which are given in terms of the position operator x_n, momentum operator p_n, and frequency $\omega^{(n)}_{\rm res}$ of the NAMR. Moreover, $\sigma^z_n = |e_n\rangle\langle e_n| - |g_n\rangle\langle g_n|$ is the Pauli Z operator for the nth TLS, while $\sigma^-_n = |g_n\rangle\langle e_n|$ ($\sigma^+_n = |g_n\rangle\langle e_n|$) is the qubit lowering (raising) operator given in terms of the ground ($|g_n\rangle$) and excited ($|e_n\rangle$) states of the nth TLS; $\omega^{(n)}_{\rm q}$ is the TLS frequency and $\omega^{(n)}_{\rm drv}$ ($\overline{\omega}^{(n)}_{\rm drv}$) is the NAMR (TLS) driving-field frequency. The coupling strengths of the subsystems, as shown in Fig. 1, are denoted by Ω_n, f_n, g_n, and J_{12}. The symbol h.c. denotes the Hermitian conjugated term.

This system, described by Eq. (1), can be realized in various ways as a combination of two types of implementations, e.g.: (i) the proposal of Ref. [43] for observing single-mode phonon blockade in a driven single NAMR coupled to a superconducting quantum two-level system and (ii) the system of two nonlinearly-coupled NAMRs, which was experimentally realized in the NTT experiments (see, e.g., Ref [54] and references therein). It is worth noting that we assumed that the interaction $H_{\rm int}$ is additionally driven at frequencies $\omega^{(1)}_{\rm drv}$ and $\omega^{(2)}_{\rm drv}$, as given in Eq. (5), which slightly generalizes the model applied in Ref. [54]. We also note that the interaction described by Eq. (4) conserves the number of excitations, in contrast to that described by Eq. (5).

B. Time-independent Hamiltonian in a rotated dressed-qubit basis

In the following, we assume the following large detunings:

$$
\begin{aligned}
\Delta^{(n)}_{\rm rq} &\equiv \omega^{(n)}_{\rm res} - \omega^{(n)}_{\rm q} = \omega^{(n)}_{\rm drv} - \overline{\omega}^{(n)}_{\rm drv} \gg g_n > 0, && (7)\\
\Delta_n &\equiv \Delta^{(n)}_{\rm rd} \equiv \omega^{(n)}_{\rm res} - \omega^{(n)}_{\rm drv} = \omega^{(n)}_{\rm q} - \overline{\omega}^{(n)}_{\rm drv} \gg \Omega_n > 0. && (8)
\end{aligned}
$$

The large detuning $\Delta^{(n)}_{\rm rq} \gg g_n$ implies that, e.g., the qubit states cannot be flipped by the interaction with the NAMR (see

Appendix A). While the large detuning $\Delta_n \gg \Omega_n$ enables us to omit, in particular, the terms which do not conserve the number of excitations in the TLS-NAMR interaction Hamiltonian, as will be explained below. Note that the assumption that $\omega_{\rm res}^{(n)} - \omega_{\rm drv}^{(n)} = \omega_{\rm q}^{(n)} - \overline{\omega}_{\rm drv}^{(n)}$ is not essential in our derivation, and is applied only for simplicity.

First, we transform the Hamiltonian H, given in Eq. (1), into a rotating reference frame by the unitary transformation

$$U_R(t) = \prod_n \exp\left(-i\omega_{\rm drv}^{(n)} a_n^\dagger a_n t - \tfrac{1}{2} i\bar{\omega}_{\rm drv}^{(n)} \sigma_n^z t\right), \quad (9)$$

which results in the following effective Hamiltonian

$$H' = U_R^\dagger H U_R - iU_R^\dagger \frac{\partial}{\partial t} U_R, \quad (10)$$

which can be given explicitly as

$$\begin{aligned} H' &= H'_{\rm res} + H'_{\rm q} + H'_{\rm JC} + H'_{\rm int}, && (11)\\ H'_{\rm res} &= \sum_n \Delta_n a_n^\dagger a_n + f_n\left(a_n + a_n^\dagger\right), && (12)\\ H'_{\rm q} &= \sum_n \frac{\Delta_n}{2}\sigma_n^z + \frac{\Omega_n}{2}\sigma_n^x, && (13)\\ H'_{\rm JC} &= \sum_n g_n[a_n\sigma_n^+ \exp(-i\Delta_{\rm rq}^{(n)} t) + {\rm h.c.}], && (14)\\ H'_{\rm int} &= J_{12}(a_1 + a_1^\dagger)(a_2 + a_2^\dagger), && (15) \end{aligned}$$

where $\sigma_n^x = \sigma_n^+ + \sigma_n^-$. Note that this Hamiltonian is still time dependent.

Now we diagonalize the qubit Hamiltonian, given by Eq. (13), by transforming it into a dressed-qubit basis following the method described in, e.g., Refs. [62, 63]. Thus, one finds

$$H''_{\rm q} = \sum_n \frac{\bar{\Delta}_n}{2}\rho_n^z, \quad (16)$$

where $\bar{\Delta}_n = \sqrt{\Delta_n^2 + \Omega_n^2}$ and the dressed-qubit operator $\rho_n^z = |E_n\rangle\langle E_n| - |G_n\rangle\langle G_n|$ can be defined by the dressed-qubit basis states [63]:

$$\begin{aligned} |E_n\rangle &= \cos x_n |e_n\rangle + \sin x_n |g_n\rangle,\\ |G_n\rangle &= -\sin x_n |e_n\rangle + \cos x_n |g_n\rangle, \end{aligned} \quad (17)$$

where $x_n = (1/2)\tan^{-1}(\Omega_n/\Delta_n)$. It is seen that the dressed nth qubit refers to the nth TLS dressed with the nth NAMR phononic field (for a general discussion see Ref. [62]).

To transform the Hamiltonian $H'_{\rm JC}$, given by Eq. (14), into the dressed-qubit basis, first we note that

$$a\sigma_n^+ = \cos^2(x_n) a\rho_n^+ - \sin^2(x_n) a\rho_n^- + \tfrac{1}{2}\sin(2x_n) a\rho_n^z, \quad (18)$$

where $\rho_n^- = |G_n\rangle\langle E_n|$, and $\rho_n^+ = |E_n\rangle\langle G_n|$. By recalling the assumption, given in Eq. (8), we can write $a\sigma_n^+ \approx \cos^2(x_n) a\rho_n^+$. For example, if $\Omega_n/\Delta_n = 0.1$ then $\cos^2(x_n) = 0.9975$, $\sin^2(x_n) = 0.0025$, and $\sin(2x_n)/2 \approx 0.05$. Thus, we can omit the second and third terms in Eq. (18), and their Hermitian conjugates, which do not conserve the number of excitations. Then, the Hamiltonian $H'_{\rm JC}$ can approximately be transformed into

$$H''_{\rm JC} \approx \sum_n g'_n[a_n\rho_n^+ \exp(-i\Delta_{\rm rq}^{(n)} t) + {\rm h.c.}], \quad (19)$$

where $g'_n = g_n \cos^2(x_n)$.

To obtain a time-independent total Hamiltonian, we transform it into a qubit rotating frame by applying the standard unitary transformation

$$U_q = \exp(-iH''_q t). \quad (20)$$

This results in

$$H'''_{\rm JC} = \sum_n g'_n \left\{a_n\rho_n^+ \exp[-i(\Delta_{\rm rq}^{(n)} - \bar{\Delta}_n)t] + {\rm h.c.}\right\}. \quad (21)$$

By assuming $\Delta_{\rm rq}^{(n)} = \bar{\Delta}_n$ (for $n = 1, 2$), one obtains the time-independent Jaynes-Cummings Hamiltonian in the dressed-qubit basis,

$$H'''_{\rm JC} = \sum_n g'_n(a_n\rho_n^+ + a_n^\dagger\rho^-). \quad (22)$$

Thus, after these transformations, the total Hamiltonian reads

$$H''' = H'''_{\rm res} + H'''_{\rm JC} + H'''_{\rm int}, \quad (23)$$

where $H'''_{\rm int} = H'_{\rm int}$ and $H'''_{\rm res} = H'_{\rm res}$. Note that $H'''_q = 0$.

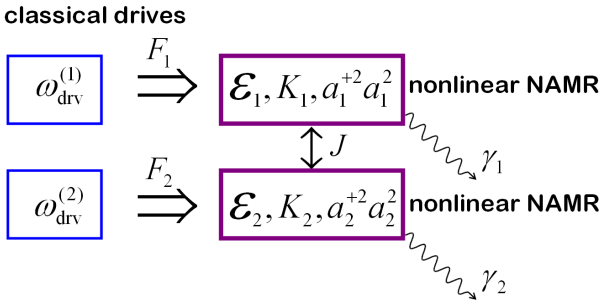

FIG. 2: (Color online) Schematic diagram for the couplings in the dissipative hybrid system described by the effective Hamiltonian given in Eq. (28), which consists of two nonlinear NAMRs driven by classical fields. Here F_n and J denote the corresponding coupling strengths; K_n is the effective Kerr nonlinearity of the nth nonlinear NAMR, and $\mathcal{E}_n$ is its energy. Other symbols are the same as in Fig. 1.

C. Effective Hamiltonian with a qubit-induced nonlinearity

We assume another large detuning

$$\delta_n \equiv \bar{\Delta}_n - \Delta_n \gg g'_n, \quad (24)$$

which leads to dispersive interactions. Note that conditions (8) and (24) are not contradictory as can be shown as follows: By denoting $r_n = \Omega_n/\Delta_n$, Eq. (24) can be given as

$$\delta_n = \Delta_n\left(\sqrt{1 + r_n^2} - 1\right) \approx \tfrac{1}{2}\Delta_n r_n^2 \gg g'_n. \quad (25)$$

Thus, Eqs. (8) and (24) can be combined as the following hierarchy of conditions:

$$\Delta_n \gg \Omega_n \gg g'_n, \quad \text{such that} \quad \Omega_n^2 \gg 2g'_n\Delta_n. \tag{26}$$

For example, if $r_n = 0.1$ then we require $0.005\Delta_n \gg g'_n$.

Now we describe how the TLS-NAMR interaction can effectively induce a Kerr-type nonlinearity. To show this, we can expand the Hamiltonian H' in a power series of the parameter

$$\lambda_n = \frac{g'_n}{\delta_n} = \frac{g_n \cos^2\left[\frac{1}{2}\tan^{-1}(\Omega_n/\Delta_n)\right]}{\sqrt{\Delta_n^2+\Omega_n^2}-\Delta_n}, \tag{27}$$

such that $|\lambda_n| \ll 1$. As derived in Appendix A, one can keep terms of such expansions up to λ_n^3 only and assume that both TLSs remain in their excited states $|E_n\rangle$ during the whole system evolution, which can be observed for the large detuning $\Delta_{\rm rq}^{(n)} \gg g_n$, as given in Eq. (7). Then, the total Hamiltonian H''', given in Eq. (23), can be transformed into the following effective Hamiltonian:

$$\begin{aligned} H_{\rm eff} &= \sum_n \left[H_{\rm Kerr}^{(n)}(0,1) - \omega_{\rm drv}^{(n)} a_n^\dagger a_n + F_n\left(a_n + a_n^\dagger\right)\right] \\ &\quad + J(a_1 + a_1^\dagger)(a_2 + a_2^\dagger), \end{aligned} \tag{28}$$

where the Kerr-type Hamiltonian

$$H_{\rm Kerr}^{(n)}(0,1) = K_n a_n^\dagger a_n^\dagger a_n a_n + \mathcal{E}_n a_n^\dagger a_n \tag{29}$$

describes an effectively nonlinear nth NAMR. Here the nth NAMR energy $\mathcal{E}_n$ and the effective Kerr nonlinearity K_n are given by

$$\mathcal{E}_n = \omega_{\rm res}^{(n)} + 2K_n + g'_n\lambda_n(1-\lambda_n^2), \tag{30}$$

$$K_n = -g'_n\lambda_n^3, \tag{31}$$

respectively. Moreover, $F_n = f_n(1+\frac{1}{2}\lambda_n^2)$ is an effective driving-field strength, and $J = J_{12}(1+\frac{1}{2}\lambda_1^2)(1+\frac{1}{2}\lambda_2^2)$ is an effective coupling between the NAMRs. All these coupling coefficients are shown in Fig. 2. A few lowest energy levels for the Kerr-type part of this Hamiltonian, given in Eq. (29), are shown in Fig. 3(a), where we set $n = 1$.

Equation (28) describes an effective driven Kerr-type self-interaction (an anharmonic model) in one phonon mode nonlinearly coupled to another phonon mode. In the context of various types of photon and phonon blockades, this phonon-phonon model can formally be considered as a two-mode generalization of the single-mode phonon model of Ref. [43]. Moreover, our model with the nonlinear coupling between the NAMRs can be interpreted as a generalization of (i) the linearly-coupled hybrid model studied in Ref. [44] to describe single-phonon and single-photon blockades and (ii) the linearly-coupled optical model with single-mode [64–66] and two-mode drivings [67, 68] leading to two-mode single-photon blockades.

The Kerr Hamiltonian, given in Eq. (29) can formally be rewritten as $(k, l = 0, 1, ...)$

$$H_{\rm Kerr}^{(n)}(k,l) = K_n(a_n^\dagger a_n - k)(a_n^\dagger a_n - l) + \mathcal{E}_n^{kl} a_n^\dagger a_n - C_n^{kl}, \tag{32}$$

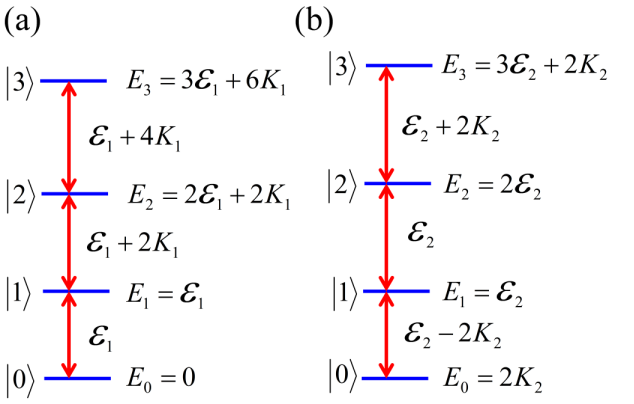

FIG. 3: (Color online) Energy levels for the Kerr-type Hamiltonians given in (a) Eq. (29) (with $n = 1$) and (b) Eq. (33) (with $n = 2$ and $\mathcal{E}_2 \equiv \mathcal{E}_2^{12}$).

where $\mathcal{E}_n^{kl} = \mathcal{E}_n + (k+l-1)K_n$, and $C_n^{kl} = klK_n$ is a constant term, which can be ignored. Thus, Eq. (32) corresponds to $H_{\rm Kerr}^{(n)}(0,1)$. In the following we will also analyze another special case of Eq. (32) corresponding to

$$H_{\rm Kerr}^{(n)}(1,2) \cong K_n(a_n^\dagger a_n - 1)(a_n^\dagger a_n - 2) + \mathcal{E}_n^{12} a_n^\dagger a_n, \tag{33}$$

where, for simplicity, the term C_n^{12} is omitted. A few lowest energy levels for this Kerr Hamiltonian are shown in Fig. 3(b), where $n = 2$ and $\mathcal{E}_2 \equiv \mathcal{E}_2^{12}$.

The driving of qubits, as given in the Hamiltonian (3), can tune the effective Kerr nonlinearity. In addition, as will be discussed in the following and was also observed in Refs. [65, 66], there is another mechanism for tuning the Kerr nonlinearity in the coupled anharmonic oscillators. Thus, even if the NAMR decay rates γ_n are much larger than the NAMR driving strengths F_n and the latter are much larger than the Kerr nonlinearities K_n, strong single-time photon/phonon antibunching can still be observed as an indicator of the photon/phonon blockade [65, 66].

We will analyze free and dissipative evolutions of the NAMR systems described by the Hamiltonian given in Eq. (28), under two different resonance conditions, as specified later in Eqs. (34) and (35).

III. PHONON BLOCKADE

A. Phonon blockade in two models

In this section we will analyze phonon blockade in two models, which are special cases of the general model described by $H_{\rm eff}$ in Eq. (28) under different resonance conditions.

In one model, we assume that the frequency $\omega_{\rm drv}^{(n)}$ of the driving field of the nth NAMR is tuned precisely to the effective free energy $\mathcal{E}_n$ $(n = 1, 2)$. Then, the effective Hamilto-

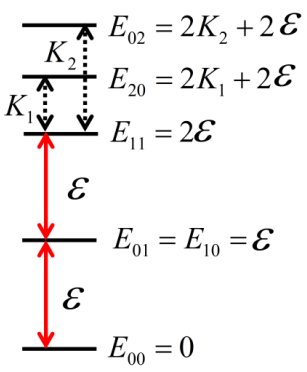

FIG. 4: (Color online) Energy levels $E_{m_1 m_2}$, given by $\bar{H}|m_1, m_2\rangle = E_{m_1 m_2}|m_1, m_2\rangle$, for the system of two uncoupled nonlinear NAMRs, described by the Hamiltonian $\bar{H} = \sum_n H^{(n)}_{\rm Kerr}$, given in Eq. (29) assuming $\mathcal{E} \equiv \mathcal{E}_1 = \mathcal{E}_2$. Here, m_1 and m_2 are the Fock states of the two NAMRs. It is seen that the levels E_{20} and E_{02} are off-resonance if $K_1, K_2 \neq \mathcal{E}/2$ and, thus, they are much less occupied than the other shown levels. This explains the occurrence of phonon blockade in this coupled system.

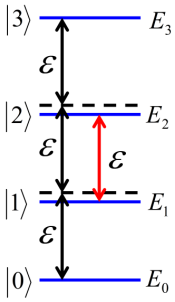

FIG. 5: (Color online) Energy levels for a single NAMR, as a simplified version of model 2: How to induce a three-phonon resonant transition in a single nonlinear NAMR described by the Hamiltonian given in Eq. (33). If the driving field frequency is resonant with the transition between the energy levels $|1\rangle$ and $|2\rangle$, $E_2 - E_1 = \mathcal{E}$, then one can also induce the three-phonon transition between the energy levels $|0\rangle$ and $|3\rangle$, since $E_3 - E_0 = 3\mathcal{E}$. Solid (dashed) lines denote real (virtual) energy levels. We note that only single-phonon transitions can be observed if the driving field frequency is tuned with the transition between other levels $|n\rangle$ and $|n+1\rangle$ ($n \neq 1$). Moreover, we cannot observe such multiphonon transitions if the system is described by the Hamiltonian given in Eq. (29) for any n.

nian $H_{\rm eff}$, given in Eq. (28), simplifies to

$$H'_{\rm eff} = \sum_n K_n a_n^\dagger a_n (a_n^\dagger a_n - 1) + \sum_n F_n \left(a_n + a_n^\dagger\right) + J(a_1 + a_1^\dagger)(a_2 + a_2^\dagger), \quad (34)$$

which is referred here to as *model 1*. The occurrence of single-phonon blockade in this model is explained in Fig. 4.

In another model, we set the frequency $\omega^{(n)}_{\rm drv}$ of the driving field of the first (second) NAMR to be tuned with the effective free energy $\mathcal{E}''_1 = \mathcal{E}_1$ ($\mathcal{E}''_2 = \mathcal{E}_2 + 2K_2$). Thus, the effective Hamiltonian $H_{\rm eff}$ reduces to:

$$H''_{\rm eff} = K_1 a_1^\dagger a_1 (a_1^\dagger a_1 - 1) + K_2 (a_2^\dagger a_2 - 1)(a_2^\dagger a_2 - 2) + \sum_n F_n \left(a_n + a_n^\dagger\right) + J(a_1 + a_1^\dagger)(a_2 + a_2^\dagger), \quad (35)$$

which is referred here to as *model 2*. Note that we ignored in Eq. (35) the irrelevant constant terms C^{kl}_n (for $n = 1, 2$). Some lowest energy levels for the Kerr-type Hamiltonian of Eq. (35) for $n = 1$ are shown in Fig. 3(a) in comparison with those for $n = 2$ shown in Fig. 3(b). A closer analysis of Fig. 3(b) shows that $E_3 - E_0 = 3\mathcal{E}$, which implies that a three-phonon resonant transition can be observed, as shown in Fig. 5. The occurrence of multiphonon blockade in this coupled system can clearly be understood by analyzing Fig. 6.

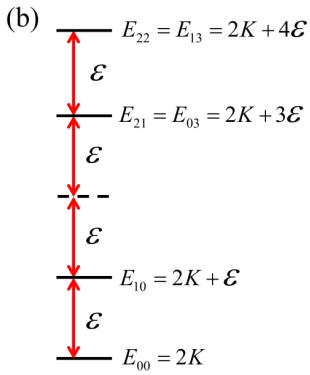

FIG. 6: (Color online) Energy levels for model 2, i.e., for the NAMR system described by the Hamiltonian $H''_{\rm eff}$, given in Eq. (35), assuming two drives and the same Kerr nonlinearities $K_1 = K_2 \equiv K$ and free energies $\mathcal{E}_1 = \mathcal{E}_2 \equiv \mathcal{E}$ of both NAMRs. This graph explains the occurrence of multiphonon blockade in this coupled system. The occurrence of the resonant three-phonon transition is explained in Fig. 5. We note that, in particular, the following levels are off-resonance: $E_{01} = \mathcal{E} \neq E_{10}$, $E_{12} = 3\mathcal{E} \neq E_{21}$, $E_{02} = E_{11} = 2\mathcal{E} \neq E_{10} + \mathcal{E}$, and $E_{20} = 2\mathcal{E} + 4K \neq E_{10} + \mathcal{E}$.

B. Phonon blockade in non-dissipative systems

In order to show phonon blockade in the non-dissipative model 1, we start from the analysis of the system, described by the Hamiltonians $H'_{\rm eff}$, without dissipation. Hereafter we assume that both NAMRs were initially in the ground phonon states, $|\psi(t = 0)\rangle = |00\rangle$. A generalization of such solution for other initial states is simple. For simplicity, we assume that both NAMRs are driven equally with the strength $F_1 = F_2 \equiv F$. Then, under these assumptions, the solution of the Schrödinger equation for the wave function $|\psi\rangle = \exp(-iH'_{\rm eff}t)|00\rangle$ is given by

$$|\psi\rangle = c_{00}|00\rangle + c_{01}|01\rangle + c_{10}|10\rangle + c_{11}|11\rangle, \quad (36)$$

with the time-dependent probability amplitudes:

$$\begin{aligned} c_{00} &= \frac{1}{4}e^{-i(2F+J)t}\left(1+e^{4iFt}+2e^{2i(F+J)t}\right), \\ c_{01} &= c_{10} = -\frac{i}{2}\exp(-iJt)\sin(2Ft), \\ c_{11} &= c_{00}-\exp(iJt), \end{aligned} \tag{37}$$

as calculated for simplicity in the two-qubit Hilbert space. Only for short evolution times, these solutions approximate well our precise numerical solutions, which were obtained in a high-dimensional Hilbert space and plotted in the left frames of Fig. 7. Much better agreement with these precise numerical solutions can be found by diagonalizing the Hamiltonian $H'_{\rm eff}$ in a two-qutrit Hilbert space. Unfortunately, we cannot obtain a compact-form analytical solution in this case, as discussed in Appendix B.

As a measure of the quality of phonon blockade (or phonon truncation), one can calculate the fidelity, defined as $F(t) = \sum_{m_1,m_2=0,1}|c_{m_1,m_2}|^2$, where the probabilities $|c_{m_1,m_2}|^2$ are computed precisely in a large-dimensional Hilbert space. For the same parameters as in the left frames of Fig. 7, we find that the fidelity periodically oscillates between the values 0.977 and 1. This shows that the evolution of phonons in the NAMRs is practically confined in a two-qubit Hilbert space in model 1 even without dissipation.

Let us now analyze phonon blockade in the non-dissipative model 2. For simplicity, we again assume that the driving field strengths are the same, $F_1 = F_2 \equiv F$. The solution of the Schrödinger equation for the wave function $|\psi\rangle = \exp(-iH''_{\rm eff}t)|00\rangle$ reads,

$$\begin{aligned} |\psi\rangle &= c_{00}|00\rangle + c_{03}|03\rangle + c_{10}|10\rangle \\ &\quad + c_{13}|13\rangle + c_{21}|21\rangle + c_{22}|22\rangle, \end{aligned} \tag{38}$$

where the probability amplitudes can be found only numerically, as explained in Appendix B. We plotted the evolution of these probability amplitudes for model 2 in Fig. 8 (solid blue curves) in analogy to those shown in Fig. 7 for model 1.

Analogously to model 1, we can quantify the quality of phonon blockade in model 2 by calculating the fidelity $F(t) = \sum_{(m_1,m_2)}|c_{m_1,m_2}|^2$; but now $(m_1,m_2) = (0,0),(0,3),(1,0),(1,3),(2,1),(2,2)$. For the dissipation-free evolution shown in Fig. 8, we find that the fidelity $F(t) \in [0.9643, 1]$. Thus, we can conclude that the evolution of phonons in the NAMRs according to model 2 even without damping is effectively confined in the Hilbert space of an entangled qutrit-quartit system.

C. Phonon blockade in dissipative systems

In the standard description of dissipation under Markov's approximation, the evolution of the reduced density operator

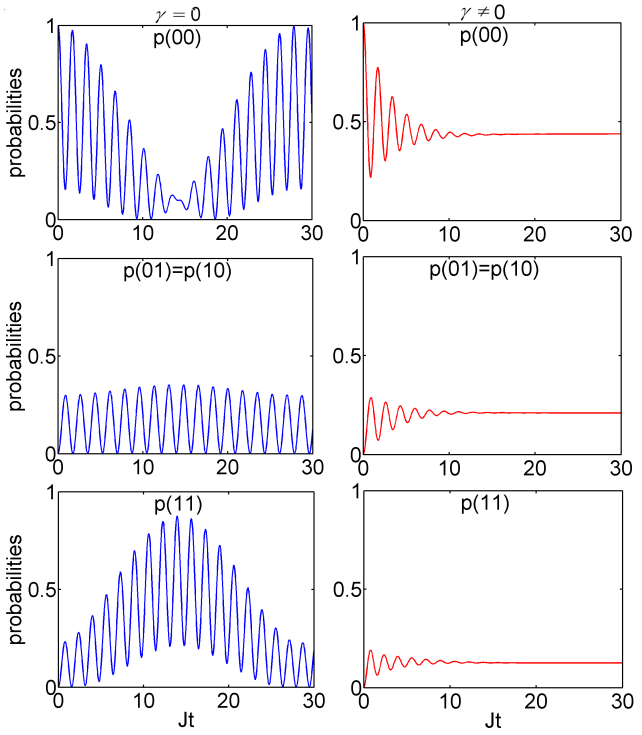

FIG. 7: (Color online) Non-stationary phonon blockade in model 1: Evolutions of probabilities $P(m_1,m_2) = |c_{m_1,m_2}|^2$ for the non-dissipative (left frames, $\gamma = 0$) and dissipative (right frames, $\gamma = J/3$) systems of the two nonlinear NAMRs described by the effective Hamiltonian $H'_{\rm eff}$ plotted for the rescaled time Jt, where J is the interaction strength between the NAMRs. Probabilities $P(m_1,m_2)$ for the other values of m_1, m_2 are negligible on the scale of these figures and, thus, not presented here. We set the Kerr nonlinearities $K_n = 10J$, the drive strengths $F_n = J$, and the mean number of thermal phonons $\bar{n}^{(n)}_{\rm th} = 0.01$ (right frames), for $n = 1, 2$. It is seen in the right frames that the oscillations are rapidly damped. Surprisingly, the stationary damped states are highly nonclassical as it is shown in other figures.

$\rho(t)$ is governed by the master equation,

$$\begin{aligned} \dot{\rho} &= -i[H_{\rm eff},\rho] \\ &\quad + \sum_n \frac{\gamma_n}{2}\bar{n}^{(n)}_{\rm th}(2a_n^\dagger\rho a_n - a_n a_n^\dagger\rho - \rho a_n a_n^\dagger) \\ &\quad + \sum_n \frac{\gamma_n}{2}(\bar{n}^{(n)}_{\rm th}+1)(2a_n\rho a_n^\dagger - a_n^\dagger a_n\rho - \rho a_n^\dagger a_n), \end{aligned} \tag{39}$$

where γ_n is the nth NAMR decay rate (damping constant), $\bar{n}^{(n)}_{\rm th} = \{\exp[\omega/(k_BT)]-1\}^{-1}$ is the mean number of thermal phonons interacting with the nth NAMR, k_B is the Boltzmann constant, and T is the reservoir temperature at thermal equilibrium. For simplicity, we assume equal decay rates $\gamma_1 = \gamma_2 \equiv \gamma$ and mean thermal-phonon numbers $\bar{n}^{(1)}_{\rm th} = \bar{n}^{(2)}_{\rm th} \equiv \bar{n}_{\rm th}$. In our numerical analysis, we focus on the steady-state solutions $\rho_{\rm ss} = \rho(t\to\infty)$ of the master equation, obtained for $\dot{\rho} = 0$. We obtain such numerical solutions by applying the inverse power method implemented in Ref. [69].

Examples of dissipative evolutions of phonon-number

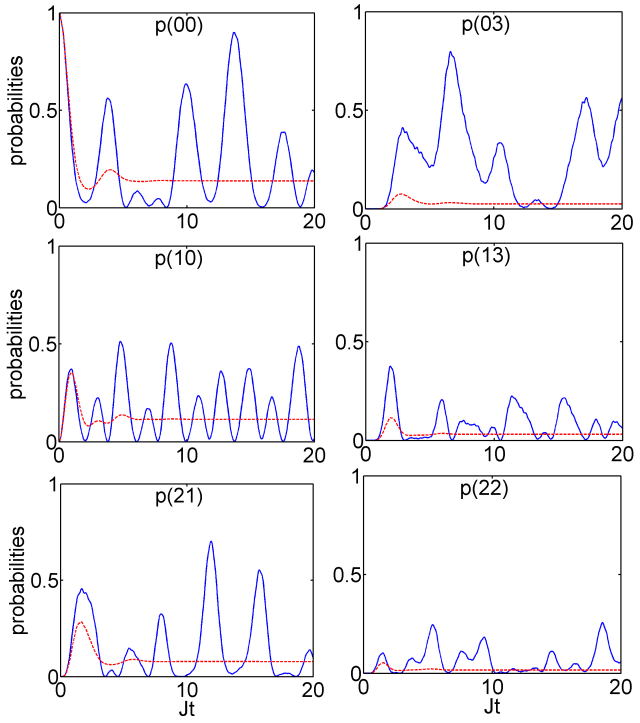

FIG. 8: (Color online) Non-stationary phonon blockade in model 2: Probabilities $P(m_1, m_2)$ same as in Fig. 7 but for the non-dissipative (blue solid curves, $\gamma = 0$) and dissipative (red dashed curves, $\gamma = J/3$) NAMR systems described by the effective Hamiltonian $H''_{\rm eff}$.

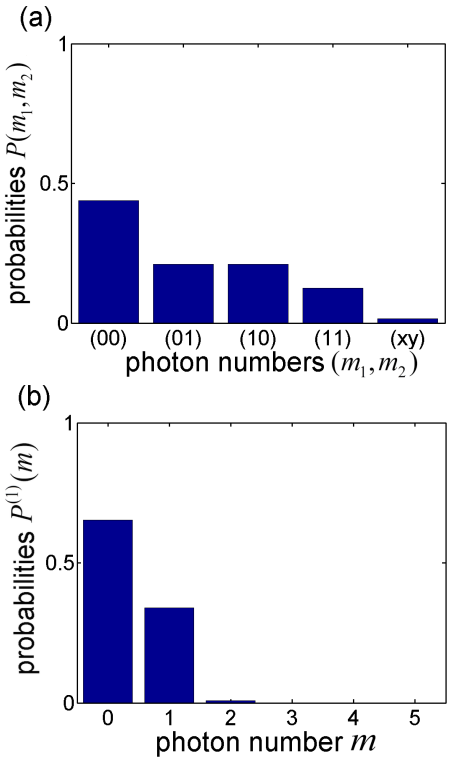

FIG. 9: (Color online) Stationary solutions for model 1 describing an effective two-qubit system and, thus, corresponding to single-phonon blockade: The phonon-number probabilities (a) $P(m_1, m_2) = \langle m_1, m_2|\rho_{\rm ss}|m_1, m_2\rangle$ for two NAMRs and (b) $P^{(1)}(m) = \langle m|{\rm Tr}_2(\rho_{\rm ss})|m\rangle$ for the first NAMR (and, equivalently, $P^{(2)}(m)$ for the second NAMR) for the steady-state solutions $\rho_{\rm ss}$ of the master equation (39) with the Hamiltonian $H'_{\rm eff}$, given by Eq. (34), assuming the same parameters as in Fig. 7. Moreover, (xy) denotes all phonon numbers such that $x, y > 1$, so $P(xy) = 1 - \sum_{m_1,m_2=0,1} P(m_1, m_2)$. Panel (b) shows single-phonon blockade in every NAMR.

probabilities are shown by the red curves in Fig. 7 for model 1 and the red dashed curves in Fig. 8 for model 2. It is seen that short-time oscillations are rapidly damped. The resulting steady-state phonon-number probabilities are shown in Figs. 9 and 10, respectively. In panels (a) of these figures, we plotted the probabilities $P(m_1, m_2) = \langle m_1, m_2|\rho_{\rm ss}|m_1, m_2\rangle$ for the two-NAMR density matrices $\rho_{\rm ss}$. While in panels (b) and (c), we presented the single-NAMR phonon-number probabilities $P^{(n)}(m) = \langle m|\rho^{(n)}_{\rm ss}|m\rangle$ for $\rho^{(n)}_{\rm ss} = {\rm Tr}_{3-n}(\rho_{\rm ss})$, with $n = 1, 2$.

We can clearly interpret these results as single-, two-, and three-phonon blockades corresponding to the cases shown in Figs. 9(b), 10(b), and 10(c), respectively.

We note that the steady states are not pure, contrary to the standard assumptions made in analogous studies of single-photon blockades of optical [66, 68] and optomechanical [58] systems. Indeed for the examples of the states shown in Figs. 9 and 10, we found that their purities are the following: ${\rm Tr}\rho^2_{\rm ss} = 0.4212$ and ${\rm Tr}(\rho^{(1)}_{\rm ss})^2 = {\rm Tr}(\rho^{(2)}_{\rm ss})^2 = 0.5670$ for model 1, and ${\rm Tr}\rho^2_{\rm ss} = 0.1471$, ${\rm Tr}(\rho^{(1)}_{\rm ss})^2 = 0.3920$, and ${\rm Tr}(\rho^{(2)}_{\rm ss})^2 = 0.3212$ for model 2.

Finally we note that, for simplicity, we applied here the standard master equation, given by Eq. (39) assuming two separable dissipation channels for the NAMRs. A more precise description, which could be especially important for a stronger coupling between the NAMRs, should be based on a generalized master equation within the general formalism of Breuer and Petruzzione (see sect. 3.3 in Ref. [70]). In this approach both NAMRs dissipate into usually-entangled dissipation channels. An explicit form of such generalized master equation for two strongly-coupled infinitely-dimensional systems will be presented elsewhere [71]. Note that a generalized master equation for an infinitely-dimensional system strongly coupled to a qubit system has already been well studied [72].

IV. PHONON BLOCKADE IN PHASE SPACE

Here we apply the Wigner function $W \equiv W^{(0)}$ and the Cahill-Glauber s-parametrized quasiprobability distribution (QPD) $W^{(s)}$ in order to visualize the nonclassical properties of the phonon-blockaded states studied in Sec. III.

The Wigner function for a two-mode (or two-NAMR) state

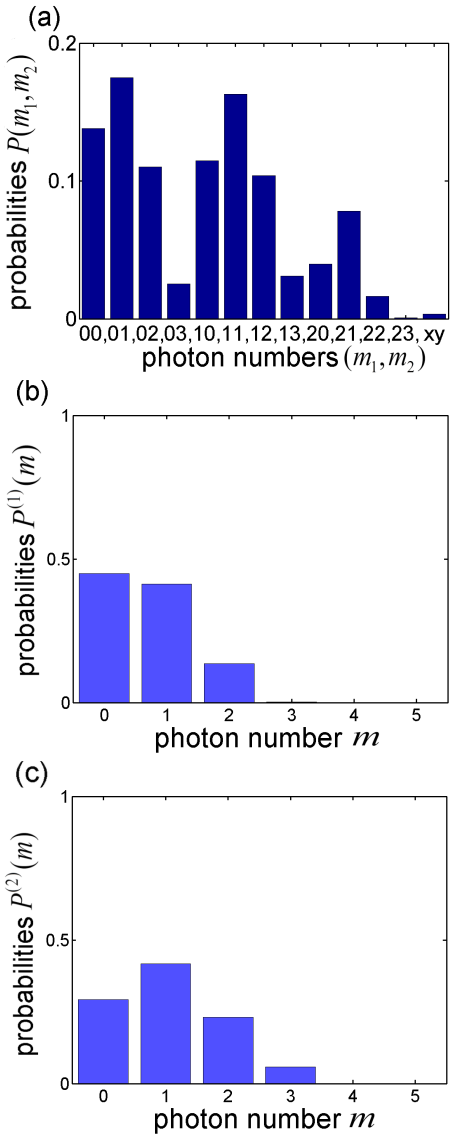

FIG. 10: (Color online) Stationary solutions for model 2 describing an effective qutrit-quartit system and, thus, corresponding to multiphonon blockade: The phonon-number probabilities (a) $P(m_1,m_2) = \langle m_1,m_2|\rho_{\rm ss}|m_1,m_2\rangle$ for two NAMRs, and (b,c) $P^{(n)}(m) = \langle m|{\rm Tr}_{3-n}(\rho_{\rm ss})|m\rangle$ for the nth NAMR ($n = 1,2$) for the steady-state solutions $\rho_{\rm ss}$ of the master equation (39) with the Hamiltonian $H''_{\rm eff}$, given by Eq. (35), and the same parameters as in Fig. 7 and (xy) denotes all phonon numbers such that $x > 2$ and $y > 3$. Panel (b) [(c)] shows two-phonon (three-phonon) blockade in the first (second) NAMR.

ρ can be given by

$$W_{12}(\alpha_1,\alpha_2) = W_{12}(q_1,p_1,q_2,p_2) = \frac{1}{\pi^2}\int \langle q_1-x_1,q_2-x_2|\rho|q_1+x_1,q_2+x_2\rangle \times \exp\left[2i(p_1x_1+p_2x_2)\right]dx_1dx_2, \quad (40)$$

in terms of the canonical position q_n and momentum p_n operators, and $\alpha_n = q_n + ip_n$ for the nth NAMR. It is seen that Eq. (40) is a straightforward generalization of the Wigner function for a single-mode (in our case single-NAMR) case,

$$W(\alpha_n) = W(q_n,p_n) = \frac{1}{\pi}\int \langle q_n-x_n|\rho_n|q_n+x_n\rangle \times \exp\left(2ip_nx_n\right)dx_n, \quad (41)$$

where ρ_n can correspond, e.g., to ${\rm Tr}_{3-n}\rho$ for $n = 1,2$. Specifically, the single-NAMR Wigner function $W(\alpha_n)$ can be considered as the marginal functions of the two-NAMR Wigner function $W(\alpha_1,\alpha_2)$.

Figure 11 shows the Wigner function $W(\alpha_1) = W(\alpha_2)$ for the steady state $\rho_{\rm ss}^{(n)} = {\rm Tr}_{3-n}\rho_{\rm ss}$ ($n = 1,2$) for some chosen values of the coupling and damping parameters. Unfortunately, the contribution of the vacuum state in $\rho_{\rm ss}$ is dominant, as shown in Fig. 9. Thus, the Wigner function for $\rho_{\rm ss}^{(n)}$ looks like a slightly deformed Gaussian representing the vacuum.

To show this deformation more clearly we also plotted the s-parametrized Cahill-Glauber QPD, $W^{(s)}(\alpha_n)$ for $s = 1/2$. For simplicity, we analyze this QPD only for a single-mode (i.e., single-NAMR) case, while the extension for the two- and multi-mode cases is straightforward. The Cahill-Glauber QPD $W^{(s)}(\alpha_n)$ can be defined in the Fock-state representation of an arbitrary-dimensional single-mode state ρ as follows [73]:

$$W^{(s)}(\alpha_n) = \sum_{k,l=0}^{\infty}\langle k|\rho|l\rangle\langle l|T^{(s)}(\alpha_n)|k\rangle, \quad (42)$$

where

$$\langle l|T^{(s)}(\alpha_n)|k\rangle = c\sqrt{\frac{l!}{k!}}y^{k-l+1}z^l(\alpha_n^*)^{k-l}L_l^{k-l}(x_{\alpha_n}), \quad (43)$$

for $s \in [-1,1]$, $c = \frac{1}{\pi}\exp[-2|\alpha_n|^2/(1-s)]$, $x_{\alpha_n} = 4|\alpha_n|^2/(1-s^2)$, $y = 2/(1-s)$, $z = (s+1)/(s-1)$, and L_l^{k-l} are the associate Laguerre polynomials. As for the Wigner function, α_n is a complex number, where its real and imaginary parts can be interpreted as canonical position and momentum, respectively. The operator $T^{(s)}(\alpha_n)$ is defined in the Fock representation by Eq. (43). In the special cases of $s = -1,0,1$, the QPD $W^{(s)}(\alpha_n)$ becomes the Husimi Q, Wigner W, and Glauber-Sudarshan P functions, respectively.

Here, we apply a well known definition of nonclassicality (see, e.g., Ref. [74] and references therein): A photonic or phononic state can be considered nonclassical if and only if its Glauber-Sudarshan P function is not positive (semi)definite, which means that it is not a classical probability density. Thus only coherent states and their statistical mixtures are classical.

The Wigner functions and $1/2$-parametrized QDPs for the steady states of models 1 and 2 are shown in Figs. 11 and 12, respectively. These steady states $\rho_{\rm ss}$ are nonclassical, as they correspond to the partially-incoherent finite superpositions of phonon Fock states, which are not mixtures of coherent states (in particular, they are not the vacuum). The nonclassicality of these states $\rho_{\rm ss}$ is clearly seen in the non-positive functions $W^{(s=1/2)}$ (their negative regions are plotted in blue). However, the nonclassicality of $\rho_{\rm ss}$ is difficult to deduce from the plots of the nonnegative Wigner functions.

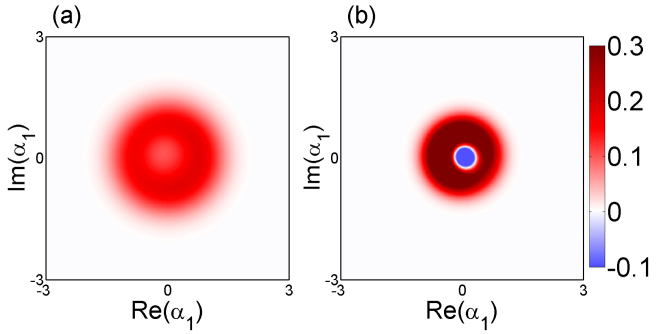

FIG. 11: (Color online) Stationary solutions for model 1 as in Fig. 11 but for (a) the single-NAMR Wigner function $W(\alpha_1) = W(\alpha_2)$ and (b) the single-NAMR quasiprobability distribution (QPD) function $W^{(s)}(\alpha_1) = W^{(s)}(\alpha_2)$ with parameter $s = 1/2$ for the steady-state solutions $\rho_{\rm ss}^{(n)} = {\rm Tr}_{3-n}\rho_{\rm ss}$ (for $n = 1, 2$). Note that the negative regions of the QPD functions are marked in blue.

To understand this apparent discrepancy, we recall a known relation between two single-mode QPDs, $\mathcal{W}^{(s_0)}$ and $\mathcal{W}^{(s)}$ for the chosen parameters $s < s_0$ [73]:

$$\mathcal{W}^{(s)}(\alpha_n) = c' \int \exp\left(-\frac{2|\alpha_n - \beta_n|^2}{s_0 - s}\right) \mathcal{W}^{(s_0)}(\beta_n) {\rm d}^2\beta_n, \tag{44}$$

where $c' = 2/[\pi(s_0 - s)]$. This relation means that any QPD for $s \leq s_0$ can be obtained from $\mathcal{W}^{(s_0)}$ by mixing it with the Gaussian noise. In particular, the Wigner function can be obtained in this way from the $P = \mathcal{W}^{(1)}$ and $\mathcal{W}^{(1/2)}$ QPDs. By decreasing the parameter s from $s_0 = 1$, the QPD $\mathcal{W}^{(s)}$, for a given nonclassical state, becomes less and less negative, and finally becomes nonnegative at some $s' \geq -1$. As a result, in the analyzed examples shown in Figs. 11 and 12, the negativity of the P-function for $\rho_{\rm ss}$ is only partially lost in the QPDs $\mathcal{W}^{(1/2)}$, but completely lost in the corresponding Wigner functions.

V. ENTANGLEMENT, DIMENSIONALITY, AND NONCLASSICALITY OF NAMRS

To analyze more deeply the nonclassical properties of the generated phonon states in the two NAMRs in models 1 and 2, we apply the following measures of quantum correlations: the negativity and its closely related entanglement dimensionality, as well as the entanglement potential, as a measure of nonclassicality.

A. Entanglement

To quantify the entanglement of a bipartite state ρ of arbitrary finite dimensions, we apply the negativity N, which can be expressed as [75]

$$N(\rho) = \frac{||\rho^\Gamma||_1 - 1}{2} \tag{45}$$

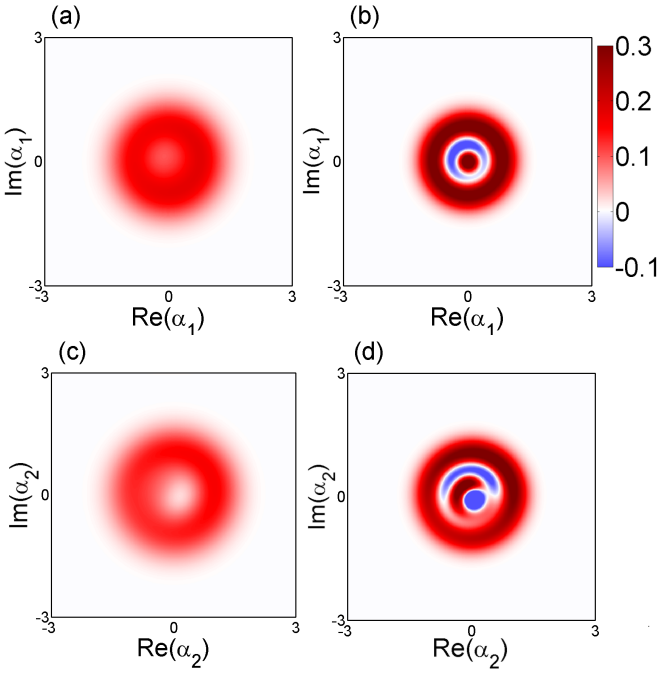

FIG. 12: (Color online) Stationary solutions for model 2 as in Fig. 11, but for the single-NAMR Wigner functions $W(\alpha_n)$ (a,c) and the single-NAMR QPD functions $W^{(s)}(\alpha_n)$ with parameter s=1/2 (b,d) for the steady-state solutions $\rho_{\rm ss}^{(n)} = {\rm Tr}_{3-n}\rho_{\rm ss}$ (for $n = 1, 2$).

via the trace norm $||\rho^\Gamma||_1$ of the partially-transposed statistical operator ρ^Γ. This entanglement measure is closely related to the Peres-Horodecki criterion. The negativity N is an entanglement monotone and, thus, can be used in quantifying entanglement in bipartite systems. However, the negativity does not detect bound entanglement (i.e., nondistillable entanglement) in systems more complicated than two qubits or qubit-qutrit [75]. The negativity can be interpreted operationally. For example, the logarithmic negativity,

$$E_{\rm cost}(\rho) = \log_2[N(\rho) + 1], \tag{46}$$

quantifies the entanglement cost under operations preserving the positivity of the partial transpose (PPT), which is, for short, referred to as the PPT entanglement cost [76, 77].

The evolutions of this entanglement measure are plotted in Fig. 13(a) for model 1 and Figs. 14(a) for model 2, by including and excluding the dissipation. The oscillations of $E_{\rm cost}(\rho)$ are rapidly damped; however the entanglement is not completely lost in the infinite-time limit. Indeed, for the coupling parameters K, J, F, decay rate γ, and thermal-phonon mean numbers $\bar{n}_{\rm th}$ specified in the figures, the entanglement between the NAMRs is found to be $E_{\rm cost}(\rho_{\rm ss}) = 0.1413$ for model 1 and almost three times smaller $E_{\rm cost}(\rho_{\rm ss}) = 0.0494$ for model 2.

B. Dimensionality

The negativity also determines the dimensionality $D_{\rm ent}$ of entanglement, which is the number of degrees of freedom of two entangled subsystems. Specifically, the entanglement dimensionality $D_{\rm ent}$ for a bipartite state ρ is simply related to the negativity $N(\rho)$ as follows [78]

$$D_{\rm ent}(\rho) = 2N(\rho) + 1 = ||\rho^{\Gamma}||_1. \tag{47}$$

More precisely, the least integer $\geq D_{\rm ent}$ gives a lower bound to the number of entangled dimensions between the entangled subsystems of ρ [78]. According to Eq. (47), $D_{\rm ent} = 1$ for separable states ($N = 0$). This measure could be useful for characterizing even a single test system (in our case, a single phonon mode) with unknown quantum dimension. This can be done in a standard way "by entangling [the test system] with an auxiliary system of known dimension and measuring the negativity, a lower bound to the number of quantum levels in the test system can be found" [78]. In our case of two NAMRs, we can directly apply the negativity, without the use of an auxiliary system, to determine a lower bound to the number of quantum levels in the total system (see also Ref. [79]).

The evolutions of the entanglement dimensionality are plotted in Fig. 13(b) for model 1 and Fig. 14(b) for model 2. Since the entanglement dimensionality and the entanglement cost are closely related, we can conclude, the same as for $E_{\rm cost}(\rho)$, that $D_{\rm ent}$ does vanish in the steady states. Specifically, the entanglement dimensionality between the NAMRs reads: $D_{\rm ent}(\rho_{\rm ss}) = 1.2058$ for model 1 and $D_{\rm ent}(\rho_{\rm ss}) = 1.0696$ for model 2.

C. Nonclassicality

The negativity can also be used in quantifying the nonclassicality of a single-mode photonic or phononic state ρ_n via the so-called entanglement potential (EP), which is defined as [74, 80]

$$\mathrm{EP}(\rho_n) \equiv \log_2 \left\{ N\left[\exp(-iHt)(\rho_n \otimes |0\rangle\langle 0|) \exp(iHt) \right] + 1 \right\}. \tag{48}$$

Here $H = \frac{1}{2}(a_n^\dagger b + a_n b^\dagger)$ describes a balanced beam splitter or a linear coupler, where a_n and b are the annihilation operators of the input modes. The basic idea behind this measure in optics is as follows: If a single-mode nonclassical (classical) photonic state is combined with the vacuum at a beam splitter then the output state is entangled (separable), for which various entangled measures (including the negativity) can be applied. By generalizing this concept for phonons it is enough to interpret this ancilla beam splitter as a linear coupler.

The evolutions of the nonclassicality of single NAMRs are plotted in Fig. 13(c) for model 1 and Figs. 14(c) and 14(d) for model 2. We find the following nonzero values of $\mathrm{EP}(\rho_{\rm ss}^{(n)})$ in the corresponding steady states: $\mathrm{EP}(\rho_{\rm ss}^{(1)}) = \mathrm{EP}(\rho_{\rm ss}^{(2)}) = 0.1126$ for model 1, while $\mathrm{EP}(\rho_{\rm ss}^{(1)}) = 0.1354$ for the first NAMR and $\mathrm{EP}(\rho_{\rm ss}^{(1)}) = 0.1770$ for the second NAMR in model 2.

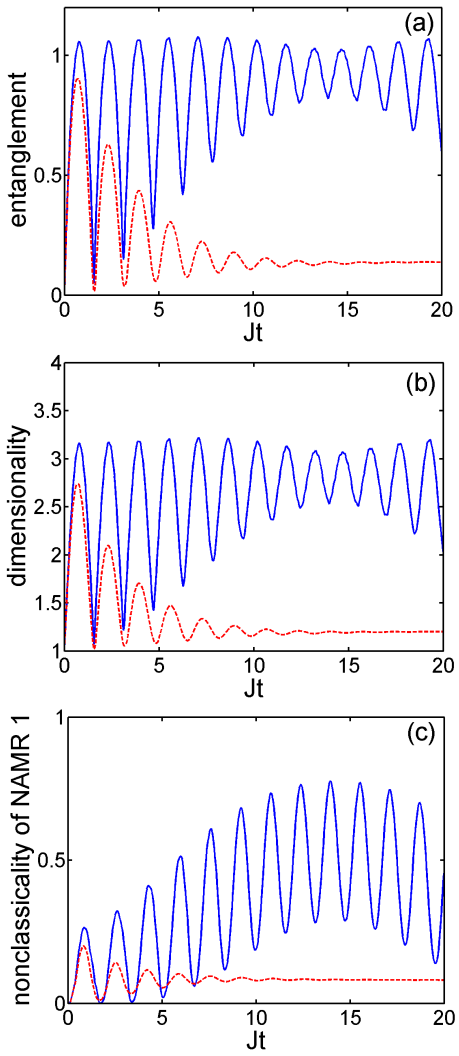

FIG. 13: (Color online) Non-stationary solutions for model 1: (a) Entanglement, measured by the PPT entanglement cost $E_{\rm cost}(\rho)$, (b) dimensionality of entanglement $D_{\rm dim}(\rho)$, and (c) nonclassicality, measured by the entanglement potential $\mathrm{EP}(\rho^{(1)})$, of the first (and, equivalently, second) NAMR for the states ρ generated in the non-dissipative (blue solid upper curves, $\gamma = 0$) and dissipative (red dashed lower curves, $\gamma = J/3$) systems described by the effective Hamiltonian $H'_{\rm eff}$. Parameters are same as in Fig. 7.

Here, for brevity, we studied only the evolution of one nonclassicality measure. In future work, it might be physically interesting to compare it with the evolution of other measures [74] and witnesses [81] of nonclassicality.

VI. DISCUSSION AND CONCLUSIONS

We studied tunable phonon blockade, which can be intuitively understood as follows: Any number of phonons can be generated in a harmonic resonator. However, this is not possible in an anharmonic resonator, which is characterized by nonlinear (nonequidistant) energy levels. So, if the driv-

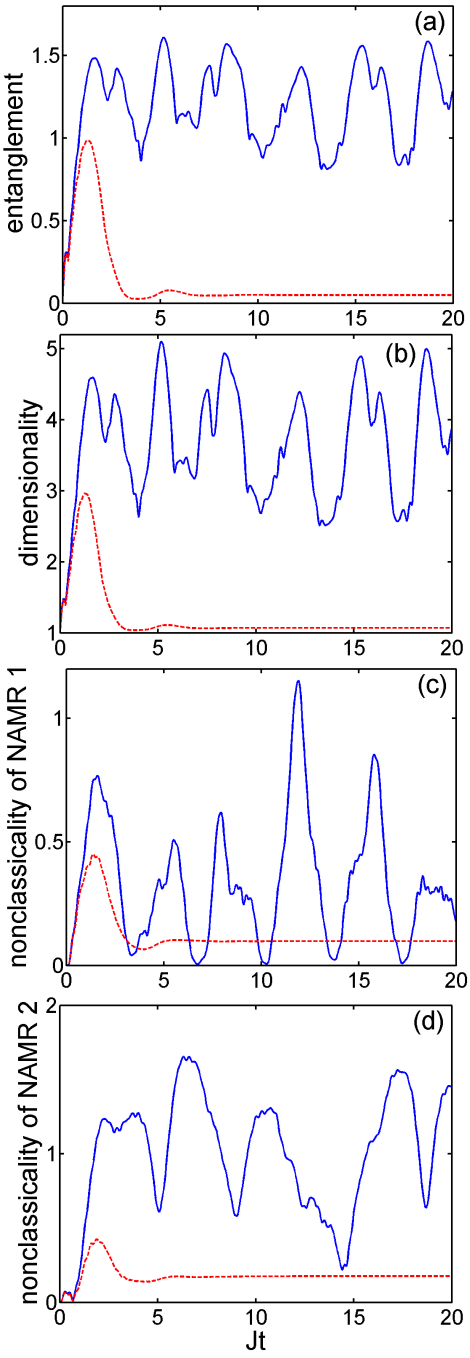

FIG. 14: (Color online) Non-stationary solutions for model 2: Same as in Fig. 13 but for the effective Hamiltonian $H''_{\rm eff}$. Additionally, panel (d) shows the nonclassicality, measured by the entanglement potential $\mathrm{EP}(\rho^{(2)})$, of the second NAMR.

ing field is in resonance with the transition between the two lowest levels (say $|0\rangle$ and $|1\rangle$), then it is not in resonance with the transitions between the other levels. Thus, single-phonon blockade can be observed. We showed in detail that a higher-order n-phonon blockade can also be observed in a dissipative nonlinear system if the driving field is resonant with the transition between other levels $|0\rangle$ and $|n\rangle$. By applying coupled nonlinear systems, instead of a single system, one can more easily tune various types of multi-phonon two-mode blockades, as studied in detail in this paper.

It is important to clarify the main differences between our model of coupled oscillators and that studied in, e.g., Refs. [44, 65, 66]: (1) Here we assumed that the oscillators are nonlinearly coupled as described by the Hamiltonian $H_{\rm int} \sim (a_1 + a_1^\dagger)(a_2 + a_2^\dagger)$ in contrast to the linear coupling given by $H_{\rm int} \sim (a_1^\dagger a_2 + a_1 a_2^\dagger)$, which was applied in Refs. [44, 65, 66]. Note that this linear coupler (which is formally equivalent to a beam splitter or a frequency converter), does not change the nonclassicality of a total system [74]. In contrast to this, the nonlinear coupler increases the nonclassicality of a total system, as measured by, e.g., the entanglement potential. It is also worth noting that, by applying our precise numerical calculations, we found the steady-states of the NAMRs to be only partially coherent (partially mixed), while the steady states calculated in, e.g., Ref. [66] were assumed to be completely coherent (perfectly pure). (2) We have derived an effective Kerr-type Hamiltonian from a microscopic one, given in Eqs. (1), while an analogous Kerr-type Hamiltonian in Refs. [44, 65, 66] was assumed without derivation. Moreover, we studied here the Kerr interaction under two different resonance conditions, as described by Eqs. (29) and (33). Refs. [44, 65, 66] discussed only the Kerr interaction given by Eq. (29). (3) We analyzed the blockade of mechanical phonons, contrary to photon blockade studied in Refs. [65, 66]. Moreover, the interplay between single-phonon blockade in one oscillator and single-photon blockade in another oscillator was studied in Ref. [44]. Here we predicted tunable k-phonon blockades (with $k = 1, 2, 3$) in each oscillator, where the k-phonon Fock state impedes the excitation of more phonons. To our knowledge, multiphonon blockade has not been studied before.

In conclusion, we showed here a rich tapestry of phonon blockade effects in two coupled nonlinear nanomechanical resonators. Different types of phonon blockade could be "picked out" of this tapestry by controlling the nonlinearity via ancilla TLS, and by changing the driving frequency of the resonators themselves. Within these different types of phonon blockade, the coupled NAMRs can be made to behave like two coupled qubits, a qutrit coupled to a quartit, or even two coupled qudits. We verified this picture by looking at the nonclassical properties of these states including their single-NAMR nonclassicality, and two-NAMR entanglement and entanglement dimensionality. The nonclassical properties of these states were also analyzed in phase space by applying the s-parametrized Cahill-Glauber quasiprobability distributions and, in particular, the Wigner function. We expect that, if realized in experiment, the ability to operate in these different regimes will have a range of applications in quantum information and quantum technologies.

Acknowledgement

A.M. was supported by the Polish National Science Centre under the grants No. DEC-2011/02/A/ST2/00305 and No.

DEC-2011/03/B/ST2/01903. A.M. acknowledges a long-term fellowship from the Japan Society for the Promotion of Science (JSPS). Y.X.L. was supported by the National Natural Science Foundation of China under Grant No. 61328502, the National Basic Research Program of China (973 Program) under Grant No. 2014CB921401, the Tsinghua University Initiative Scientific Research Program, and the Tsinghua National Laboratory for Information Science and Technology (TNList) Cross-discipline Foundation. J.B. was supported by the Palacký University under the Project No. IGA-PřF-2015-02. F.N. was partially supported by the RIKEN iTHES Project, the MURI Center for Dynamic Magneto-Optics via the AFOSR award number FA9550-14-1-0040, the IMPACT program of JST, and a Grant-in-Aid for Scientific Research (A).

Appendix A: Derivation of the effective Hamiltonian

Here we show how to derive the effective Hamiltonian $H_{\rm eff}$, given by Eq. (28), from the Hamiltonian H''', given in Eq. (23). The latter can be divided into the following parts:

$$H''' = H'''_{\rm sys} + H'''_{\rm drv} + H'''_{\rm int}, \tag{A1}$$

where

$$H'''_{\rm sys} = H'''_0 + H'''_{\rm JC} = \sum_n \Delta_n a_n^\dagger a_n + H'''_{\rm JC}, \tag{A2}$$

$$H'''_{\rm drv} = \sum_n f_n(a + a^\dagger). \tag{A3}$$

Here $H'''_{\rm JC}$ is given by Eq. (22) and $H'''_{\rm int} = H'_{\rm int}$ is given by Eq. (15).

Our derivation is based on the method described in Ref. [82] for the exact diagonalization of the Jaynes-Cummings model with the following unitary transformation

$$U_n = \exp[-\Lambda(\lambda_n)(a_n^\dagger \rho_n^- - a_n \rho_n^+)], \tag{A4}$$

where the operator $\Lambda(\lambda_n) = -\arctan(2\lambda_n\sqrt{N_n})/(2\sqrt{N_n})$ is given in terms of the total number of excitations $N_n = a_n^\dagger a_n + |E_n\rangle\langle E_n|$ in the nth NAMR and TLS. Thus, the expansions of the annihilation operators, $\bar{a}_n = U_n^\dagger a U_n$ and $\bar{\rho}_n^- = U_n^\dagger \rho_n^- U_n$ of Ref. [82] can be rewritten for our dressed qubit states as follows:

$$\bar{a}_n = a_n(1 + \tfrac{1}{2}\lambda_n^2\rho_n^z) + \lambda_n h_n^{(3)}\rho_n^- + \lambda_n^3 a_n^2 \rho_n^+ + \mathcal{O}(\lambda_n^4), \tag{A5}$$

$$\bar{\rho}_n^- = h_n^{(1)}\rho_n^- + \lambda_n a_n \rho_n^z - \lambda_n^2 a_n^2 \rho_n^+ + \mathcal{O}(\lambda_n^3), \tag{A6}$$

where $h_n^{(k)} = 1 - k\lambda_n^2(a_n^\dagger a_n + 1/2)$ and $\mathcal{O}(\lambda_n^k)$ denotes the omitted terms of order $\sim \lambda_n^k$ and higher. Now one can easily transform the Hamiltonian H''' into

$$\bar{H} = U_1^\dagger U_2^\dagger H''' U_2 U_1. \tag{A7}$$

In particular, by applying Eq. (A5), $H'''_{\rm drv}$ transforms into

$$\bar{H}_{\rm drv} = \sum_n f_n[\bar{a}_n + \bar{a}^\dagger]. \tag{A8}$$

If the qubits remain in the excited dressed-qubit states $|E_n\rangle$, given in Eq. (17), then

$$\langle E_1E_2|\bar{H}_{\rm drv}|E_1E_2\rangle = \sum_n f_n(a_n + a_n^\dagger)(1 + \lambda_n^2/2) + \mathcal{O}(\lambda_n^4). \tag{A9}$$

The assumption of a "frozen" state of both qubits is physically justified for the large detuning $\Delta_{\rm rq}^{(n)} \gg g_n$, as specified in Eq. (7). Moreover, $H'''_{\rm int}$ transforms into

$$\bar{H}_{\rm int} = J_{12}(\bar{a}_1 + \bar{a}_1^\dagger)(\bar{a}_2 + \bar{a}_2^\dagger), \tag{A10}$$

and, thus,

$$\langle E_1E_2|\bar{H}_{\rm int}|E_1E_2\rangle = J(a_1 + a_1^\dagger)(a_2 + a_2^\dagger) + \mathcal{O}(\lambda_n^4), \tag{A11}$$

where $J = J_{12}(1 + \lambda_1^2/2)(1 + \lambda_2^2/2)$. Analogously, by generalizing the results of Ref. [82] for the dressed-qubit operators ρ_n^z, one can find that

$$\begin{aligned}\bar{H}_{\rm sys} &= U^\dagger H'''_{\rm sys} U - iU^\dagger \frac{\partial}{\partial t} U \\ &= H'''_0 - \tfrac{1}{2}\sum_n \delta_n\big(1 - \sqrt{1 + 4N_n\lambda_n^2}\big)\rho_n^z \\ &\approx H'''_0 + \sum_n 2K_n a_n^\dagger a_n + h_n\rho_n^z + K_n(a_n^\dagger)^2 a_n^2 \rho_n^z,\end{aligned} \tag{A12}$$

where H'''_0 is defined in Eq. (A2), $h_n = \chi_n(a_n^\dagger a_n + \frac{1}{2})$, with $\chi_n = g'_n\lambda_n(1 - \lambda_n^2)$, and the effective Kerr nonlinearity reads $K_n = -g'_n\lambda_n^3 = -(g'_n)^4/\delta_n^3$. Moreover, $U = U_1U_2$ and $\frac{\partial}{\partial t}U = 0$. Thus, one can write

$$\begin{aligned}\langle E_1E_2|\bar{H}_{\rm sys}|E_1E_2\rangle &= \sum_n C_n + D_n a_n^\dagger a_n \\ &\quad + K_n(a_n^\dagger)^2 a_n^2 + \mathcal{O}(\lambda_n^4),\end{aligned} \tag{A13}$$

where $C_n = (\chi_n + \bar{\Delta}_n)/2$ and $D_n \equiv \mathcal{E}_n - \omega_{\rm drv}^{(n)} = \Delta_n + 2K_n + \chi_n$. Finally, the effective Hamiltonian

$$H_{\rm eff} \equiv \langle E_1E_2|(\bar{H}_{\rm sys} + \bar{H}_{\rm drv} + \bar{H}_{\rm int})|E_1E_2\rangle, \tag{A14}$$

is given explicitly by Eq. (28), where the terms $\sim \mathcal{O}(\lambda_n^4)$ are omitted.

Appendix B: Probability amplitudes in Eqs. (36) and (38)

The probability amplitudes $c_{xy}(t) = \langle xy|\psi(t)\rangle$ (for $x, y = 0, ..., 3$), given in Eqs. (36) and (38), can be obtained using the eigenvalue decompositions $H'_{\rm eff}|E'_n\rangle = E'_n|E'_n\rangle$, as

$$c_{xy}(t) = \sum_n \exp(-iE'_n t)\langle E'_n|00\rangle\langle xy|E'_n\rangle, \tag{B1}$$

and analogously for $H''_{\rm eff}|E''_n\rangle = E''_n|E''_n\rangle$. To simplify these problems, let us limit the dimension of the Hilbert space to that of two qutrits and assume $K_1 = K_2 = 10J$ and $J =$

$F_1 = F_2$ (as in Figs. 7 and 8). Then the Hamiltonians, given in Eqs. (34) and (35), reduce to

$$\frac{H'_{\rm eff}}{J} = \begin{pmatrix} 0 & 1 & 0 & 1 & 1 & 0 & 0 & 0 & 0 \\ 1 & 0 & \sqrt{2} & 1 & 1 & \sqrt{2} & 0 & 0 & 0 \\ 0 & \sqrt{2} & 20 & 0 & \sqrt{2} & 1 & 0 & 0 & 0 \\ 1 & 1 & 0 & 0 & 1 & 0 & \sqrt{2} & \sqrt{2} & 0 \\ 1 & 1 & \sqrt{2} & 1 & 0 & \sqrt{2} & \sqrt{2} & \sqrt{2} & 2 \\ 0 & \sqrt{2} & 1 & 0 & \sqrt{2} & 20 & 0 & 2 & \sqrt{2} \\ 0 & 0 & 0 & \sqrt{2} & \sqrt{2} & 0 & 20 & 1 & 0 \\ 0 & 0 & 0 & \sqrt{2} & \sqrt{2} & 2 & 1 & 20 & \sqrt{2} \\ 0 & 0 & 0 & 0 & 2 & \sqrt{2} & 0 & \sqrt{2} & 40 \end{pmatrix}, \tag{B2}$$

$$\frac{H''_{\rm eff}}{J} = \begin{pmatrix} 20 & 1 & 0 & 1 & 1 & 0 & 0 & 0 & 0 \\ 1 & 0 & \sqrt{2} & 1 & 1 & \sqrt{2} & 0 & 0 & 0 \\ 0 & \sqrt{2} & 0 & 0 & \sqrt{2} & 1 & 0 & 0 & 0 \\ 1 & 1 & 0 & 20 & 1 & 0 & \sqrt{2} & \sqrt{2} & 0 \\ 1 & 1 & \sqrt{2} & 1 & 0 & \sqrt{2} & \sqrt{2} & \sqrt{2} & 2 \\ 0 & \sqrt{2} & 1 & 0 & \sqrt{2} & 0 & 0 & 2 & \sqrt{2} \\ 0 & 0 & 0 & \sqrt{2} & \sqrt{2} & 0 & 40 & 1 & 0 \\ 0 & 0 & 0 & \sqrt{2} & \sqrt{2} & 2 & 1 & 20 & \sqrt{2} \\ 0 & 0 & 0 & 0 & 2 & \sqrt{2} & 0 & \sqrt{2} & 20 \end{pmatrix}, \tag{B3}$$

respectively. It is seen that the matrices, given by Eqs. (B2) and (B3), differ only in their diagonal terms. Unfortunately, even in these special cases, it is very unlikely that exact analytical compact-form solutions of these eigenvalue problems can be found, as they require finding the roots of sixth and ninth order equations, respectively. Especially, highly-irregular oscillations of $c_{xy}(t)$ for model 2, as shown in Fig. 8, confirm this conclusion.

[1] X. M. H. Huang, C. A. Zorman, M. Mehregany, and M. L. Roukes, Nanoelectromechanical systems: Nanodevice motion at microwave frequencies, Nature (London) **421**, 496 (2003).

[2] R. G. Knobel and A. N. Cleland, Nanometre-scale displacement sensing using a single electron transistor, Nature (London) **424**, 291 (2003).

[3] M. P. Blencowe, Nanomechanical Quantum Limits, Science **304**, 56 (2004).

[4] M. D. LaHaye, O. Buu, B. Camarota, and K. C. Schwab, Approaching the quantum limit of a nanomechanical resonator, Science **304**, 74 (2004).

[5] M. P. Blencowe, Quantum electromechanical systems, Phys. Rep. **395**, 159 (2004).

[6] K. C. Schwab and M. L. Roukes, Putting Mechanics into Quantum Mechanics, Phys. Today **58** (7), 36, (2005).

[7] K. L. Ekinci and M. L. Roukes, Nanoelectromechanical systems, Rev. Sc. Inst. **76**, 061101 (2005).

[8] M. Aspelmeyer, T. J. Kippenberg, and F. Marquardt, Cavity Optomechanics, Rev. Mod. Phys. **86**, 1391 (2014).

[9] C. Caves, K. Thorne, R. Drever, V. D. Sandberg, and M. Zimmermann, On the measurement of a weak classical force coupled to a quantum-mechanical oscillator, Rev. Mod. Phys. **52**, 341 (1980).

[10] M. F. Bocko and R. Onofrio, On the measurement of a weak classical force coupled to a harmonic oscillator: Experimental progress, Rev. Mod. Phys. **68**, 755 (1996).

[11] E. Buks and B. Yurke, Mass detection with a nonlinear nanomechanical resonator, Phys. Rev. E **74**, 046619 (2006).

[12] V. B. Braginsky and F. Ya. Khalili, *Quantum Measurements* (Cambridge University Press, Cambridge, England, 1992).

[13] A. D. O'Connell *et al.*, Quantum ground state and single-phonon control of a mechanical resonator, Nature (London) **464**, 697 (2010).

[14] A. N. Cleland, *Foundations of Nanomechanics* (Springer, Berlin, 2003).

[15] J. D. Teufel, D. Li, M. S. Allman, K. Cicak, A. J. Sirois, J. D. Whittaker, and R. W. Simmonds, Circuit cavity electromechanics in the strong-coupling regime, Nature (London) **471**, 204 (2011).

[16] J. Chan, T.P. Mayer-Alegre, A. H. Safavi-Naeini, J. T. Hill, A. Krause, S. Gröblacher, M. Aspelmeyer, and O. Painter, Laser cooling of a nanomechanical oscillator into its quantum ground state, Nature (London) **478**, 89 (2011).

[17] A. H. Safavi Naeini, J. Chan, J. T. Hill, T. P. Mayer Alegre, A. Krause, and O. Painter, Observation of Quantum Motion of a Nanomechanical Resonator, Phys. Rev. Lett. **108**, 033602 (2012).

[18] E. Verhagen, S. Deleglise, S. Weis, A. Schliesser, and T. J. Kippenberg, Quantum-coherent coupling of a mechanical oscillator to an optical cavity mode, Nature (London) **482**, 63 (2012).

[19] K. Stannigel, P. Rabl, A.S. Sørensen, P. Zoller, and M.D. Lukin, Optomechanical transducers for long-distance quantum communication, Phys. Rev. Lett. **105**, 220501 (2010).

[20] T. A. Palomaki, J. W. Harlow, J. D. Teufel, R. W. Simmonds, and K. W. Lehnert, Coherent state transfer between itinerant microwave fields and a mechanical oscillator, Nature (London) **495**, 210 (2013).

[21] P. Huang, P. Wang, J. Zhou, Z. Wang, C. Ju, Z. Wang, Y. Shen, C. Duan, and J. Du, Demonstration of Motion Transduction Based on Parametrically Coupled Mechanical Resonators, Phys. Rev. Lett. **110**, 227202 (2013).

[22] H. Fu, T. H. Mao, Y. Li, J. F. Ding, J. D. Li, and G. Cao, Optically mediated spatial localization of collective modes of two

coupled cantilevers for high sensitivity optomechanical transducer, Appl. Phys. Lett. **105**, 014108 (2014).

[23] M. Wallquist, K. Hammerer, P. Rabl, M. Lukin, and P. Zoller, Hybrid quantum devices and quantum engineering, Phys. Scr. **2009**, 014001 (2009).

[24] A. H. Safavi-Naeini and O. Painter, Proposal for an optomechanical traveling wave phonon-photon translator, New J. Phys. **13**, 013017 (2011).

[25] C. A. Regal, J. D. Teufel, and K. W. Lehnert, Measuring nanomechanical motion with a microwave cavity interferometer, Nat. Phys. **4**, 555 (2008).

[26] M. J. Woolley, G. J. Milburn, and C. M. Caves, Nonlinear quantum metrology using coupled nanomechanical resonators, New J. Phys. **10**, 125018 (2008).

[27] L. Tian and H. J. Carmichael, Quantum trajectory simulations of two-state behavior in an optical cavity containing one atom, Phys. Rev. A **46**, R6801 (1992).

[28] W. Leoński and R. Tanaś, Possibility of producing the one-photon state in a kicked cavity with a nonlinear Kerr medium, Phys. Rev. A **49**, R20 (1994).

[29] A. Miranowicz, W. Leoński, S. Dyrting, and R. Tanaś, Quantum state engineering in finite-dimensional Hilbert space, Acta Phys. Slovaca **46**, 451 (1996).

[30] A. Imamoğlu, H. Schmidt, G. Woods, and M. Deutsch, Strongly Interacting Photons in a Nonlinear Cavity, Phys. Rev. Lett. **79**, 1467 (1997).

[31] M. J. Werner and A. Imamoğlu, Photon-photon interactions in cavity electromagnetically induced transparency, Phys. Rev. A **61**, 011801 (1999).

[32] R. J. Brecha, P. R. Rice, and M. Xiao, N two-level atoms in a driven optical cavity: Quantum dynamics of forward photon scattering for weak incident fields, Phys. Rev. A **59**, 2392 (1999).

[33] S. Rebić, S. M. Tan, A. S. Parkins, and D. F. Walls, Large Kerr nonlinearity with a single atom, J. Opt. B **1**, 490 (1999).

[34] J. Kim, O. Bensen, H. Kan, and Y. Yamamoto, A single-photon turnstile device, Nature (London) **397**, 500 (1999).

[35] S. Rebić, A. S. Parkins, and S. M. Tan, Photon statistics of a single-atom intracavity system involving electromagnetically induced transparency, Phys. Rev. A **65**, 063804 (2002).

[36] I. I. Smolyaninov, A. V. Zayats, A. Gungor, and C. C. Davis, Single-Photon Tunneling via Localized Surface Plasmons, Phys. Rev. Lett. **88**, 187402 (2002).

[37] A. J. Hoffman, S. J. Srinivasan, S. Schmidt, L. Spietz, J. Aumentado, H. E. Tureci, and A. A. Houck, Dispersive Photon Blockade in a Superconducting Circuit, Phys. Rev. Lett. **107**, 053602 (2011).

[38] C. Lang *et al.*, Observation of Resonant Photon Blockade at Microwave Frequencies Using Correlation Function Measurements, Phys. Rev. Lett. **106**, 243601 (2011).

[39] Y.X. Liu, X.W. Xu, A. Miranowicz, and F. Nori, From blockade to transparency: Controllable photon transmission through a circuit QED system, Phys. Rev. A **89**, 043818 (2014).

[40] A. Miranowicz, W. Leoński, and N. Imoto, Quantum-optical states in finite-dimensional Hilbert space. I. General formalism, Adv. Chem. Phys. **119**, 155 (2001); W. Leoński and A. Miranowicz, Quantum-optical states in finite-dimensional Hilbert space. II. State generation, Adv. Chem. Phys. **119**, 195 (2001).

[41] W. Leoński and A. Kowalewska-Kudłaszyk, Quantum scissors: Finite-dimensional states engineering, in *Progress in Optics,* edited by E. Wolf (Elsevier, Amsterdam, 2011), Vol. **56**, p. 131.

[42] K. M. Birnbaum, A. Boca, R. Miller, A. D. Boozer, T. E. Northup, and H. J. Kimble, Photon blockade in an optical cavity with one trapped atom, Nature (London) **436**, 87 (2005).

[43] Y. X. Liu, A. Miranowicz, Y. B. Gao, J. Bajer, C. P. Sun, and F. Nori, Qubit-induced phonon blockade as a signature of quantum behavior in nanomechanical resonators, Phys. Rev. A **82**, 032101 (2010).

[44] N. Didier, S. Pugnetti, Y. M. Blanter, and R. Fazio, Detecting phonon blockade with photons, Phys. Rev. B **84**, 054503 (2011).

[45] J.R. Johansson, N. Lambert, I. Mahboob, H. Yamaguchi, F. Nori, Entangled-state generation and Bell inequality violations in nanomechanical resonators, Phys. Rev. B **90**, 174307 (2014).

[46] I. Buluta, S. Ashhab, and F. Nori, Natural and artificial atoms for quantum computation, Rep. Prog. Phys. **74**, 104401 (2011).

[47] T. A. Palomaki, J. D. Teufel, R. W. Simmonds, and K. W. Lehnert, Entangling Mechanical Motion with Microwave Fields, Science **342**, 710 (2013).

[48] H. Okamoto, A. Gourgout, C. Y. Chang, K. Onomitsu, I. Mahboob, E. Y. Chang, and H. Yamaguchi, Coherent phonon manipulation in coupled mechanical resonators, Nat. Phys. **9**, 480 (2013).

[49] A. N. Cleland and M. R. Geller, Superconducting Qubit Storage and Entanglement with Nanomechanical Resonators, Phys. Rev. Lett. **93**, 070501 (2004).

[50] A. D. Armour, M. P. Blencowe, and K. C. Schwab, Entanglement and Decoherence of a Micromechanical Resonator via Coupling to a Cooper-Pair Box, Phys. Rev. Lett. **88**, 148301 (2002).

[51] L. Tian, Entanglement from a nanomechanical resonator weakly coupled to a single Cooper-pair box, Phys. Rev. B **72**, 195411 (2005).

[52] K. Jacobs and A. J. Landahl, Engineering Giant Nonlinearities in Quantum Nanosystems, Phys. Rev. Lett. **103**, 067201 (2009).

[53] S. Rips, and M. J. Hartmann, Quantum Information Processing with Nanomechanical Qubits, Phys. Rev. Lett. **110**, 120503, (2013).

[54] I. Mahboob, H. Okamoto, K. Onomitsu, and H. Yamaguchi, Two-Mode Thermal-Noise Squeezing in an Electromechanical Resonator, Phys. Rev. Lett. **113**, 167203 (2014).

[55] A. Miranowicz, M. Paprzycka, Y.X. Liu, J. Bajer, and F. Nori, Two-photon and three-photon blockades in driven nonlinear systems, Phys. Rev. A **87**, 023809 (2013).

[56] G.H. Hovsepyan, A.R. Shahinyan, and G.Y. Kryuchkyan, Multiphoton blockades in pulsed regimes beyond stationary limits, Phys. Rev. A **90**, 013839 (2014).

[57] A. Miranowicz, J. Bajer, M. Paprzycka, Y. X. Liu, A. M. Zagoskin, and F. Nori, State-dependent photon blockade via quantum-reservoir engineering, Phys. Rev. A **90**, 033831 (2014).

[58] H. Wang, X. Gu, Y. X. Liu, A. Miranowicz, and F. Nori, Tunable photon blockade in a hybrid system consisting of an optomechanical device coupled to a two-level system, Phys. Rev. A **92**, 033806 (2015).

[59] A. Faraon, I. Fushman, D. Englund, N. Stoltz, P. Petroff, and J. Vučković, Coherent generation of non-classical light on a chip via photon-induced tunnelling and blockade, Nat. Phys. **4**, 859 (2008).

[60] A. Majumdar, M. Bajcsy, and J. Vučković, Probing the ladder of dressed states and nonclassical light generation in quantum-dot-cavity QED, Phys. Rev. A **85**, 041801(R) (2012).

[61] Y. B. Gao, S. Yang, Y. X. Liu, C. P. Sun, and F. Nori, Probing Nano-Mechanical QED Effects, e-print arXiv:0902.2512.

[62] C. Cohen-Tannoudji, J. Dupont-Roc, and G. Grynberg, *Atom-Photon Interactions* (Wiley, New York, 1992).

[63] Y. X. Liu, C. P. Sun, and F. Nori, Scalable superconducting qubit circuits using dressed states, Phys. Rev. A **74**, 052321

(2006).
[64] W. Leoński and A. Miranowicz, Kerr nonlinear coupler and entanglement, J. Opt. B: Quantum Semiclass. Opt. **6**, S37 (2004).
[65] T. C. H. Liew and V. Savona, Single Photons from Coupled Quantum Modes, Phys. Rev. Lett. **104**, 183601 (2010).
[66] M. Bamba, A. Imamoglu, I. Carusotto, and C. Ciuti, Origin of strong photon antibunching in weakly nonlinear photonic molecules, Phys. Rev. A **83**, 021802(R) (2011).
[67] A. Miranowicz and W. Leoński, Two-mode optical state truncation and generation of maximally entangled states in pumped nonlinear couplers, J. Phys. B **39**, 1683 (2006);
[68] X. W. Xu and Y. Li, Tunable photon statistics in weakly nonlinear photonic molecules, Phys. Rev. A **90**, 043822 (2014).
[69] S. M. Tan, A computational toolbox for quantum and atomic optics, J. Opt. B: Quantum Semiclass. Opt. **1**, 424 (1999).
[70] H. P. Breuer and F. Petruccione, *The Theory of Open Quantum Systems* (Oxford University Press, Oxford, 2003).
[71] A. Miranowicz, N. Lambert, F. Nori *et al.*, in preparation.
[72] F. Beaudoin, J. M. Gambetta, and A. Blais, Dissipation and ultrastrong coupling in circuit QED, Phys. Rev. A 84, 043832 (2011).
[73] K. E. Cahill and R. J. Glauber, Ordered expansions in boson amplitude operators, Phys. Rev. **177**, 1857 (1969).
[74] A. Miranowicz, K. Bartkiewicz, A. Pathak, J. Perina Jr., Y. N. Chen, and F. Nori, Statistical mixtures of states can be more quantum than their superpositions: Comparison of nonclassicality measures for single-qubit states, Phys. Rev. A **91**, 042309 (2015); A. Miranowicz, K. Bartkiewicz, N. Lambert, Y. N. Chen, and F. Nori, Increasing relative nonclassicality quantified by standard entanglement potentials by dissipation and unbalanced beam splitting, Phys. Rev. A **92**, 062314 (2015).
[75] R. Horodecki, P. Horodecki, M. Horodecki, and K. Horodecki, Quantum entanglement, Rev. Mod. Phys. **81**, 865 (2009).
[76] K. Audenaert, M. B. Plenio, and J. Eisert, Entanglement Cost under Positive-Partial-Transpose-Preserving Operations, Phys. Rev. Lett. **90**, 027901 (2003).
[77] S. Ishizaka, Binegativity and geometry of entangled states in two qubits, Phys. Rev. A **69**, 020301(R) (2004).
[78] C. Eltschka and J. Siewert, Negativity as an Estimator of Entanglement Dimension, Phys. Rev. Lett. **111**, 100503 (2013).
[79] I. I. Arkhipov, J. Peřina Jr., J. Peřina, and A. Miranowicz, Comparative study of nonclassicality, entanglement, and dimensionality of multimode noisy twin beams, Phys. Rev. A **91**, 033837 (2015).
[80] J. K. Asboth, J. Calsamiglia, and H. Ritsch, Computable Measure of Nonclassicality for Light, Phys. Rev. Lett. **94**, 173602 (2005).
[81] A. Miranowicz, M. Bartkowiak, X. Wang, Y. X. Liu, and F. Nori, Testing nonclassicality in multimode fields: A unified derivation of classical inequalities, Phys. Rev. A **82**, 013824 (2010); M. Bartkowiak, A. Miranowicz, X. Wang, Y.X. Liu, W. Leoński, and F. Nori, Sudden vanishing and reappearance of nonclassical effects: General occurrence of finite-time decays and periodic vanishings of nonclassicality and entanglement witnesses, Phys. Rev. A **83**, 053814 (2011).
[82] M. Boissonneault, J. M. Gambetta, and A. Blais, Dispersive regime of circuit QED: Photon-dependent qubit dephasing and relaxation rates, Phys. Rev. A **79**, 013819 (2009).